Water Research 303 (2026) 126259

Contents lists available at ScienceDirect

Water Research

journal homepage: www.elsevier.com/locate/watres

Biodegradation of cyano liquid crystal monomers by an aerobic enrichment culture: Key degraders and interspecies synergistic mechanisms

Minghan Zhu [a,b], Chang He [c], Shaoyu Tang [a,*], Jiayu Zhang [a], Zhen Yu [a], Hui Lin [a], Yibo Yuan [b], Jonathan W.C. Wong [a], Hua Yin [b], Junfeng Niu [d], Xujun Liang [e], Zhi Dang [b]

[a] Research Center for Eco-Environmental Engineering, School of Environment and Civil Engineering, Dongguan University of Technology, Dongguan 523808, China
[b] Key Laboratory of Ministry of Education on Pollution Control and Ecosystem Restoration in Industry Clusters, School of Environment and Energy, South China University of Technology, Guangzhou, Guangdong 510006, China
[c] Guangdong-Hong Kong-Macao Joint Laboratory for Contaminants Exposure and Health, Guangdong Key Laboratory of Environmental Catalysis and Health Risk Control, Institute of Environmental Health and Pollution Control, Guangdong University of Technology, Guangzhou 510006, China
[d] State Key Laboratory of Regional Environment and Sustainability, School of Environment, Beijing Normal University, Beijing 100875, China
[e] State Key Laboratory of Soil and Water Conservation and Desertification Control, College of Natural Resources and Environment, Northwest A & F University, Yangling 712100, China

HIGHLIGHTS

- A typical CLCM-degrading enrichment was obtained from an e-waste dismantling site.
- Alkyl chain length was identified as a key factor impacting CLCM biodegradability.
- Three isolates were identified as key CLCM degraders in the enrichment culture.
- Low-abundance *G. alkanivorans* QZP3 exhibited robust typical CLCM degradation ability.
- Interspecies interactions within the enrichment underpinned efficient CLCM degradation.

GRAPHICAL ABSTRACT

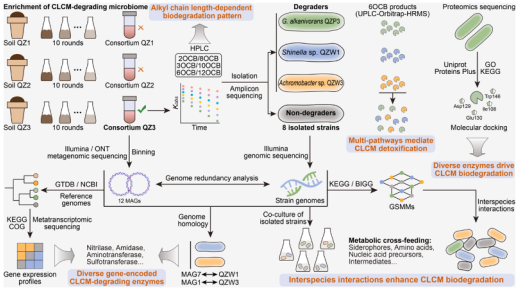

ARTICLE INFO

Keywords:
Cyano liquid crystal monomers
Bacterial enrichment culture
Functional bacteria
Biodegradation
Interspecies interactions
Molecular mechanism

ABSTRACT

Cyano liquid crystal monomers (CLCMs), as archetypal emerging contaminants, have raised global concern because of their persistence, bioaccumulation, and biotoxicity; however, their microbially mediated environmental fate remains poorly understood. Herein, we investigated the biodegradation mechanisms of typical CLCMs using an aerobic enrichment culture (QZ3) derived from e-waste-contaminated soils. Our results revealed a marked chain-length-dependent specificity in CLCM biodegradation: short-chain congeners (e.g., 4-cyano-4′-ethoxybiphenyl, 2OCB; 4-cyano-4′-propyloxybiphenyl, 3OCB) were fully degraded within 7 days; 4-cyano-4′-hexyloxybiphenyl (6OCB) achieved 99.4% removal, while 4-cyano-4′-dodecyloxybiphenyl (12OCB) showed only 30.5% degradation. We identified 19 degradation products of the model congener 6OCB, enabling us to propose a multi-pathway mechanism for the potential cascade transformation and detoxification of typical CLCMs. By integrating multi-omics profiling with culture-dependent approaches, we identified three active populations (*Gordonia alkanivorans* QZP3, *Shinella* sp. QZW1, and *Achromobacter* sp. QZW3) as the primary CLCM degraders

* Corresponding author.
E-mail address: shaoyutang@dgut.edu.cn (S. Tang).

https://doi.org/10.1016/j.watres.2026.126259
Received 24 March 2026; Received in revised form 23 May 2026; Accepted 6 June 2026
Available online 6 June 2026

in the enrichment culture QZ3. Strikingly, the low-abundance *G. alkanivorans* QZP3 harbored diverse genetic and enzymatic determinants (e.g., thiocyanate hydrolase γ-subunit, amidohydrolase, aminotransferase, cytochrome P450, and sulfotransferase) that mediated the multi-pathway transformation of CLCMs. Furthermore, extensive interspecies interactions between degraders and non-degraders, as well as among non-degraders themselves, significantly promoted CLCM biodegradation through metabolic cross-feeding of amino acids, siderophores, and nucleic acid precursors, underscoring the critical role of microbial cooperation in underpinning community-level functions. This work systematically elucidates the biodegradation mechanisms of typical CLCMs by complex microbiomes, and provides a fundamental framework for the rational design of high-performance synthetic consortia for the targeted bioremediation of emerging contaminants.

1. Introduction

Liquid crystal monomers (LCMs) are synthetic organic chemicals that serve as the key functional components in liquid crystal displays (LCDs) of electronic devices (Su et al., 2019; Zhang et al., 2025b). The rapid proliferation and short lifespan of electronic products have led to an unprecedented global e-waste crisis, with 61.9 million tons of e-waste produced in 2022 and projections exceeding 82 million tons by 2030 (Balde et al., 2024). Approximately 12.5% of this e-waste contains LCDs (Wang et al., 2024a), yet current recycling technologies cannot efficiently recover LCMs, leading to their uncontrolled release during formal disposal and informal recycling operations. Consequently, thousands of LCM congeners, predominantly cyano LCMs (CLCMs), fluorinated LCMs (FLCMs), and biphenyl analogs, have been ubiquitously detected across environmental compartments (Kong et al., 2025; Shen et al., 2022). Among these, CLCMs warrant particular scientific attention due to their widespread distribution, high bioaccumulation potential, and diverse biotoxicities (Duan et al., 2025; Feng et al., 2025; Wu et al., 2025a, 2025b; Zhang et al., 2025b). For instance, Xie et al. (2024) reported that CLCM concentrations in soils near e-waste recycling sites and LCD manufacturers were 1.7 ng g^{-1} and 0.61 ng g^{-1}, accounting for 39% and 42% of total LCMs, respectively. Jiang et al. (2024) documented that CLCMs represented over 15% of total LCMs in biological samples from the Pearl River Estuary, with accumulation ratios twice those in sediments. These findings underscore the critical need for systematic research into the environmental fate and transformation mechanisms of CLCMs.

Although photochemical oxidants (e.g., O_3 and •OH) can accelerate the degradation of LCMs (He et al., 2022; Wu et al., 2024b; Zhang et al., 2024), their effectiveness is structurally dependent. Several CLCMs, such as 4-cyano-4′-ethoxybiphenyl (2OCB), exhibit marked resistance to UV photolysis (Wu et al., 2024a), and field measurements also indicate that their atmospheric half-lives are substantially longer than model predictions (Liu et al., 2020). In contrast, microorganisms play pivotal roles in global biogeochemical cycling and are the primary drivers of natural attenuation and detoxification for most organic contaminants in the environment. For well-studied e-waste-derived pollutants such as polybrominated diphenyl ethers and polychlorinated biphenyls, decades of research have characterized diverse microbial taxa and their associated enzymes (Qi et al., 2023; Wu et al., 2024d; Zhang et al., 2022b). To date, only one study has reported the biodegradation of an FLCM (4-[difluoro (3,4,5-trifluorophenoxy) methyl]-3, 5-difluoro-4′-propylbiphenyl, DTMDPB) and identified associated genes involved in dehalogenation (*GST, nrdB*), hydroxylation (*hcaC, ubiH*), and aromatic ring cleavage (*ligB, catE*) (Zhu et al., 2024). However, the mechanisms underlying CLCM biodegradation and detoxification remain largely unknown. These knowledge gaps impede the comprehensive assessment of CLCM environmental persistence and the development of targeted bioremediation strategies.

Microbial consortia have shown great promise for eliminating recalcitrant pollutants, often outperforming single strains in efficiency and metabolic versatility. In general, consortia harbor a more diverse and comprehensive set of catabolic gene clusters, with different strains encoding key enzymes for distinct steps in complex degradation pathways, and even support simultaneous degradation of multiple pollutants (Ruan et al., 2025). Interspecies metabolic cross-feeding of nutrients (e.g., amino acids, vitamins, intermediates) tends to alleviate metabolic burdens and support the growth of key degraders, especially under oligotrophic conditions (Kost et al., 2023; Liu et al., 2025; Peng et al., 2025). Despite these advantages, elucidating the metabolic interactions within complex natural microbiomes remains challenging due to the limitations of traditional experimental methods and the restricted cultivability of environmental microbes. This challenge is further exacerbated in consortia derived from long-term enrichment cultures, where intense selective pressure creates extreme abundance skews, leaving the vast majority of species present at very low relative abundances (Peng et al., 2025; Zhang et al., 2022a). Recent advances in high-throughput sequencing, particularly long-read technologies such as Oxford Nanopore Technologies (ONT), have improved genome recovery by generating reads capable of resolving repetitive regions and assembly ambiguities (Sereika et al., 2025; Wang et al., 2021). In parallel, genome-scale metabolic models (GSMMs) and associated simulation algorithms enable *in silico* analysis of both the strain-specific metabolic potential and interspecies interactions within microbiomes (Giordano et al., 2024; Peng et al., 2025). These developments provide a crucial foundation for deciphering the mechanisms by which complex environmental microbiomes degrade emerging contaminants such as LCMs.

Herein, we developed a CLCM-degrading bacterial enrichment culture (QZ3) derived from soils collected at an e-waste-contaminated site (Fig. 1A). The main objectives of this work were to: (i) evaluate the degradation performance and substrate specificity of consortium QZ3 towards typical CLCMs with varying alkyl chain lengths; (ii) identify the major degradation products and delineate the potential cascade transformation pathways of 4-cyano-4′-hexyloxybiphenyl (6OCB), a representative CLCM selected for its widespread environmental distribution (Jiang et al., 2024; Li et al., 2022; Liu et al., 2024) and intermediate alkyl chain length; (iii) characterize the taxonomic and functional profiles of consortium QZ3 via integrated multi-omics and cultivation-dependent approaches, and pinpoint the key degraders and their potential catabolic gene repertoires; and (iv) unravel the interspecies interactions within the consortium and elucidate how these synergies drive enhanced CLCM biodegradation. Collectively, this work provides the first comprehensive mechanistic framework for understanding CLCM biodegradation by complex microbial communities.

2. Materials and methods

2.1. Chemicals, enrichment culture, and isolation of pure strains

Six CLCMs were obtained from Aladdin Biochemical Technology Co., Ltd. (Shanghai, China): 2OCB (≥ 98%), 4-cyano-4′-propyloxybiphenyl (3OCB) (≥ 97%), 6OCB (≥ 98%), 4-cyano-4′-octyloxybiphenyl (8OCB) (≥ 98%), 4′-cyano-4-decyloxybiphenyl (10OCB) (≥ 98%), and 4′-cyano-4-dodecyloxybiphenyl (12OCB) (≥ 98%). Their chemical characteristics are presented in the Supplementary Material (Table S1). Individual stock solutions of CLCMs (250 mg L^{-1}) were prepared in LC-MS grade acetonitrile (Macklin Biochemical Technology Co., Ltd., Shanghai, China). Analytical grade inorganic reagents were obtained from

Sinopharm Chemical Reagent Co., Ltd. (Shanghai, China). Ultrapure water (18.2 MΩ·cm^{-1}) was generated using a Milli-Q® IQ 7000 system (Merck KGaA, Germany). The compositions of bacterial culture media, including mineral salt medium (MSM), beef extract medium (BEM), and Luria-Bertani (LB) medium, are described in Text S1. A CLCM-degrading bacterial enrichment culture, designated as consortium QZ3, was developed from soils collected at an e-waste disassembly site (23.5481°N, 113.0465°E) in Qingyuan, China. The detailed enrichment procedure is described in Text S2. A multi-medium (LB agar, BEM agar, and MSM agar amended with 6OCB) isolation strategy was applied to maximize the recovery of cultivable strains from the consortium. Detailed procedures for the isolation, identification (16S rRNA gene sequencing), and genomic sequencing of the cultivable strains are described in Text S3 and S4.

2.2. Biodegradation assays of CLCMs

The aerobic degradation potential of the consortium QZ3 and isolated strains for 6OCB was tested using batch experiments. Specifically, pre-cultured cells (BEM, 24–48 h) were harvested by centrifugation at 8000 rpm for 6 min, washed twice with sterile MSM, and resuspended in fresh MSM. An appropriate volume of the cell suspension was inoculated into 25 mL Erlenmeyer flasks containing 10 mL of MSM with 1.0 mg L^{-1} 6OCB, achieving an initial inoculum density of 0.1 at an optical density of 600 nm (OD_{600}). To assess substrate specificity, parallel experiments were conducted using structural analogs (2OCB, 3OCB, 8OCB, 10OCB, and 12OCB) under identical conditions. We also systematically investigated the effects of key environmental parameters, including (i) initial 6OCB concentration (0.25–10.0 mg L^{-1}), (ii) inoculum density (OD_{600} = 0.01–0.3), (iii) pH (4.0–10.0), (iv) nutrient availability, and (v) co-exposure to typical e-waste-derived contaminants. The influence of nutrient availability was examined by supplementing with 500 mg L^{-1} glucose as an exogenous carbon source (Ma et al., 2020) and by imposing nitrogen limitation through the omission of the nitrogen source from MSM. Co-exposure assays were performed with representative organic pollutants [2,2′,4,4′-tetrabromodiphenyl ether (BDE-47), decabromodiphenyl ether, 3,3,5,5-tetrabromobisphenol A, 2,3′,4,4′,5-pentachlorobiphenyl (PCB118), 2,2′,3,4,4′,5,5′-heptachlorobiphenyl (PCB180), and phenanthrene (PHE)] and heavy metals [Cu(II), Pb(II), As(III), and Cd(II)], each tested individually at two concentration levels (1.0 and 5.0 mg L^{-1} for organic compounds; 5.0 and 20.0 mg L^{-1} for heavy metals) in culture medium containing 1.0 mg L^{-1} 6OCB.

Furthermore, pairwise co-cultures of eight isolated strains were conducted to investigate interspecies interactions in 6OCB biodegradation. Specifically, bacterial suspensions obtained after pre-cultivation, centrifugation, washing, and resuspension were mixed pairwise at an OD_{600} ratio of 1:1 (total OD_{600} = 0.1) and inoculated into 25 mL Erlenmeyer flasks containing 10 mL of MSM amended with 1.0 mg L^{-1}

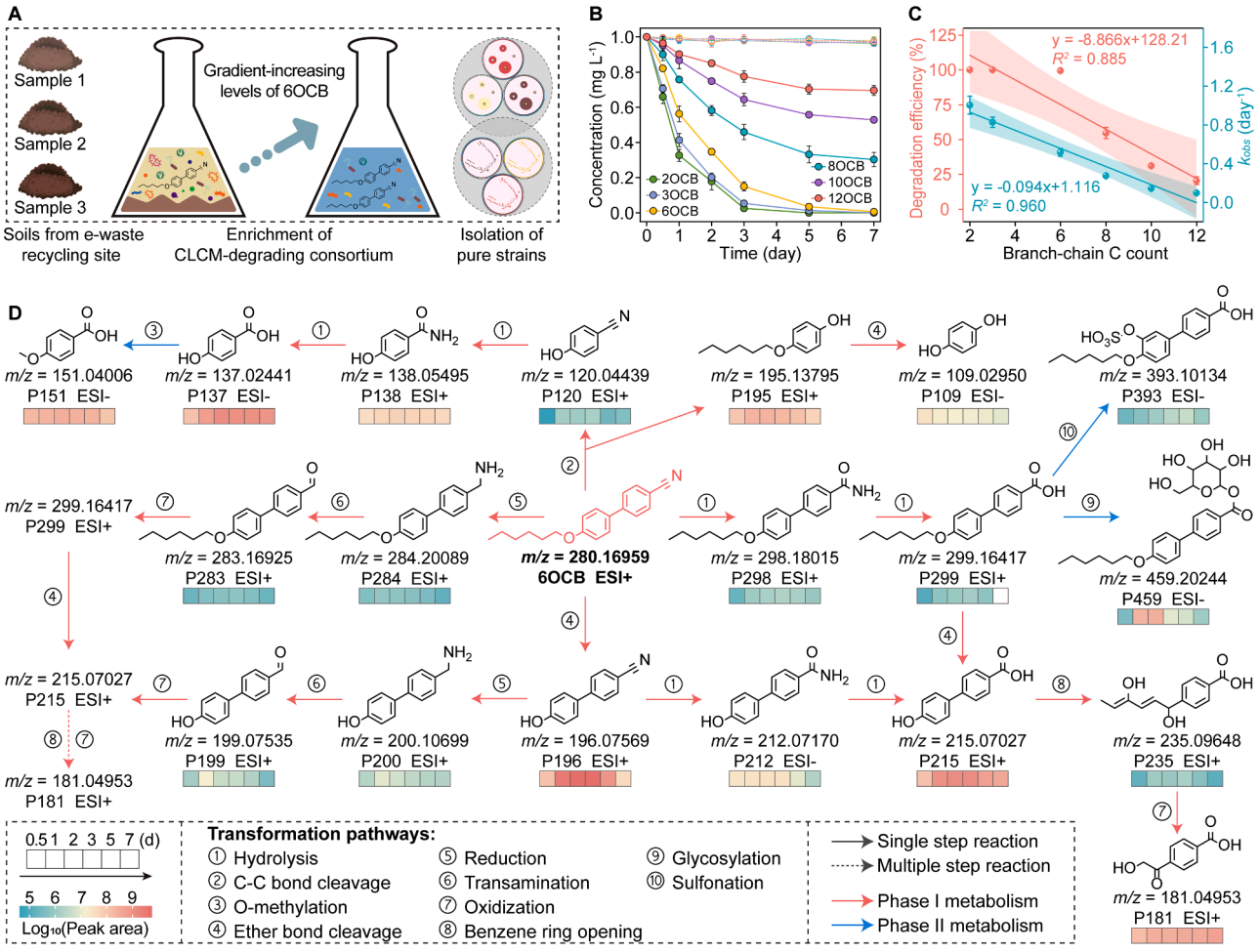

Fig. 1. Biodegradation of typical CLCMs by consortium QZ3. (A) Schematic of the "top-down" enrichment strategy for establishing the CLCM-degrading consortium. (B) Degradation kinetics of six representative CLCMs by consortium QZ3 (dashed lines represent the heat-inactivated bacterial control). (C) Correlations between the branch-chain carbon atom count of CLCMs and 7-day biodegradation efficiency (red) and 3-day biodegradation rate (green) by consortium QZ3. Data are shown as mean values ± SD (n = 3). (D) Identified products and proposed biotransformation pathways for 6OCB (recurring products show only their *m/z* and names; heatmap depicting peak area variations of products over time).

6OCB. Other experimental conditions were identical to those used in the consortium and single-strain degradation assays. All assays were performed in triplicate, and cultures were incubated in a rotary shaker at 30 °C and 160 rpm. Residual CLCMs and metabolites were analyzed via periodic destructive sampling.

2.3. Analytical methods of CLCMs and transformation products

The concentrations of the six CLCMs were quantified by high-performance liquid chromatography (HPLC; Thermo Fisher Scientific Inc., USA) with diode-array detection (DAD). The UV absorption maxima of the CLCMs were determined at 295 nm using an Evolution™ 201/220 UV–Vis Spectrophotometer (Thermo Fisher Scientific Inc., USA) (Fig. S1). Sample pretreatment procedures and instrumental conditions are provided in Text S5. The transformation products of 6OCB were screened by ultra-performance liquid chromatography coupled with a high-resolution Orbitrap mass spectrometer (UPLC—Orbitrap-HRMS) (Dionex Ultimate 3000 and Q Exactive Focus, Thermo Fisher Scientific Inc., USA) with electrospray ionization (ESI) in both positive and negative modes (Text S6), as previously described (Zhu et al., 2024). The relative quantification of identified products was performed using the peak areas of the corresponding extracted ion chromatograms from UPLC—Orbitrap-HRMS. The toxicities of typical CLCMs and 6OCB degradation products to aquatic organisms were evaluated using the Ecological Structure-Activity Relationship (ECOSAR) program (U.S. Environmental Protection Agency, Washington, DC, 2023).

2.4. Total DNA extraction and metagenomic sequencing of consortium QZ3

Fifteen samples were collected from five degradation stages (i.e., days 0, 0.5, 1, 3, and 6) during incubation with 1.0 mg L^{-1} 6OCB for Illumina sequencing (n = 3 for each stage). These samples were then pooled for ONT sequencing. Briefly, total DNA was extracted using a FastPure Soil DNA Isolation Kit (MJYH, Shanghai, China) following the manufacturer's protocols, followed by validation of genomic DNA integrity (1% agarose gel electrophoresis), purity (Nanodrop), and concentration (Qubit). For Illumina sequencing, the purified DNA was sheared to ~400 bp using Covaris M220 (Gene Company Limited, China), and paired-end libraries were constructed using the NEXTFLEX™ Rapid DNA-Seq Kit (Bioo Scientific, Austin, TX, USA), followed by sequencing on an Illumina NovaSeq 6000 platform (Illumina Inc., San Diego, CA, USA). ONT libraries were prepared using the SQK-LSK109 kit (ONT, UK) and sequenced on a PromethION R9.4 platform. Both sequencing runs were conducted at Majorbio Bio-Pharm Technology Co., Ltd. (Shanghai, China), yielding 195.48 Gbp (Illumina) and 12.73 Gbp (ONT) of raw data. The metagenome assembly and binning procedures are described in Text S7.

2.5. Total RNA extraction and metatranscriptomic sequencing of consortium QZ3

The same batch of samples utilized for Illumina metagenomic sequencing were also processed for metatranscriptomic analysis. The total RNA was extracted using the Soil Total RNA Isolation Kit (Majorbio, Shanghai, China) following the manufacturer's protocols. The purified RNA underwent standard Illumina library preparation with the Illumina® Stranded mRNA Prep Kit (Illumina, San Diego, CA, USA), followed by ribosomal RNA depletion using the RiboCop rRNA Depletion Kit (Lexogen, Vienna, Austria). Sequencing was conducted on an Illumina HiSeq 3000 platform using the HiSeq 3000/4000 PE Cluster Kit (Illumina Inc., San Diego, CA, USA) at Majorbio Bio-Pharm Technology Co., Ltd. (Shanghai, China).

The genomes of isolated strains were utilized to substitute their homologous metagenome-assembled genomes (MAGs) as reference genomes for metatranscriptomic analysis. Raw metatranscriptomic reads were quality-filtered using Fastp (v0.23.4) (Chen et al., 2018), followed by rRNA read depletion with SortMeRNA (v2.1b) (Kopylova et al., 2012). The remaining clean reads were mapped to the reference genomes using Bowtie2 (v2.5.1) (Langmead and Salzberg, 2012). The mapped reads were counted using HTseq (v0.13.5) to obtain the read count of each gene, followed by normalization to Transcripts Per Million (TPM) (Anders et al., 2015). Differentially expressed genes (DEGs) between groups were identified using the DESeq2 package (v1.34.0) (Love et al., 2014) and defined by $|\log_2$ (fold change, FC)$| > 1$ and adjusted p-value ≤ 0.05. Temporal DEGs (tDEGs) were clustered into different expression patterns based on the TPM matrix using the Mfuzz package (Lokesh and Matthias, 2007). Functional annotations of tDEGs were performed using the Clusters of Orthologous Groups (COG, https://www.ncbi.nlm.nih.gov/research/cog/) and Kyoto Encyclopedia of Genes and Genomes (KEGG, https://www.genome.jp/kegg/) databases.

2.6. Genome-scale metabolic models simulated pairwise interactions

To investigate potential metabolic exchanges among community members, GSMMs were reconstructed for each isolated strain and for their non-redundant MAGs (i.e., MAG3, MAG4, MAG6, MAG8, MAG9, MAG10, and MAG12). Specifically, genomes were initially annotated using BAKTA (v5.1) (Schwengers et al., 2021), and metabolic models were subsequently reconstructed using CarveMe (v1.5.2) (Machado et al., 2018). The quality of the reconstructed GSMMs was assessed using MEMOTE (v0.17). Subsequently, interspecies dependencies and metabolite cross-feeding potential were analyzed using SMETANA (v1.1.0) (Zelezniak et al., 2015).

2.7. Proteomic profiling and molecular docking analysis of G. alkanivorans QZP3

Pre-cultured *G. alkanivorans* QZP3 cells were inoculated into MSM with 1.0 mg L^{-1} 6OCB, with unsupplemented MSM as the blank control (CK). Each treatment was performed in triplicate, and cultures were incubated at 30 °C and 160 rpm for 48 h. Cells were harvested by centrifugation at 10,000 rpm for 6 min at 4 °C and washed three times with ice-cold Phosphate-Buffered Saline. Protein extraction, tryptic digestion and Data-Independent Acquisition Mass Spectrometry (DIA-MS) were conducted by Majorbio Bio-Pharm Technology Co., Ltd. (Shanghai, China) (Xu et al., 2025a). Raw DIA data were imported into Spectronaut (v18) software for database searching. The *Gordonia alkanivorans* reference proteome from the UniProt Knowledgebase (Taxonomy ID: 84,096, https://www.uniprot.org/taxonomy/84096) was used as the search database. The search parameters were set as follows: Protein FDR ≤ 0.01; Peptide FDR ≤ 0.01; Peptide Confidence $\geq 99\%$; XIC width ≤ 75 ppm. Protein quantification was performed using the MaxLFQ algorithm. The t-test function in R was used to calculate the significance of differences (p-value) and FC between groups. Differentially expressed proteins (DEPs) were identified with thresholds of FC > 1.2 (upregulated) and adjusted p-value < 0.05. Principal component analysis was used to reveal overall differences in protein expression across samples. The biological functions and pathway distributions of DEPs were annotated and enriched against the KEGG and Gene Ontology (GO) databases.

Molecular docking simulations were conducted to characterize the binding interactions between 6OCB and its major intermediates with the potential 6OCB-catabolizing proteins. Briefly, the three-dimensional (3D) structures of the ligand molecules were retrieved from the PubChem database (https://pubchem.ncbi.nlm.nih.gov/) or produced using Chem3D (v22.2.0), and then converted to PDB format with OpenBabel (v3.1.1) (O'Boyle et al., 2011). AlphaFold-generated 3D structures of target proteins were acquired from the UniProt Knowledgebase linked to the AlphaFold Protein Structure Database. Following structural optimization of both ligands and macromolecules, docking was performed

with AutoDockTools 1.5.7 using the Lamarckian Genetic Algorithm (LGA) (El-Hachem et al., 2017; Xing et al., 2023). The conformation with the lowest binding energy was selected for analysis. Hydrogen bonding and hydrophobic interactions were visualized using Discovery Studio 4.5 Client and PyMOL 2.6.

3. Results and discussion

3.1. Degradation performance and transformation pathways of typical CLCMs

The consortium QZ3 exhibited distinct structural specificity in degrading the six CLCMs (Fig. 1B). Specifically, after 7 days of incubation, 2OCB and 3OCB were completely degraded, and 6OCB was removed with 99.4% efficiency. However, the degradation efficiency decreased markedly with increasing alkyl chain length, reaching 69.6% for 8OCB, 47.2% for 10OCB, and 30.5% for 12OCB. For comparison, Zhu et al. (2024) reported that culture BG1 achieved 67.5% degradation of the FLCM (DTMDPB) at an initial concentration of 0.5 mg L^{-1} after 10 days of incubation. The correlation analyses demonstrated significant negative correlations between the number of alkyl chain carbon atoms and both the degradation efficiency ($R^2 = 0.885$) and degradation rate ($R^2 = 0.960$) (Fig. S2 and Fig. 1C), indicating that the alkyl chain length exerts a critical regulatory effect on CLCM biodegradability. However, the detailed molecular mechanisms underlying this chain-length dependence, including hydrophobicity-driven differences in cellular uptake, steric constraints at enzyme active sites, and differential cytotoxicity, have not been definitively established. Further structural biology and purified enzyme kinetic studies are required to confirm causality. Additionally, 6OCB was selected as a representative substrate to investigate the key factors governing biodegradation. Dose-response assays revealed that increasing the initial 6OCB concentration from 1.0 to 10 mg L^{-1} markedly reduced the degradation efficiency from 99.4% to 34.4% (Fig. S3A), suggesting that high CLCM doses may inhibit the consortium's metabolic activity and growth. Inoculum dosage (OD_{600}) and solution pH also significantly affected 6OCB degradation, with the optimal performance achieved at an inoculum $OD_{600} \geq 0.1$ under near-neutral pH conditions (Fig. S3B–C). Notably, several co-occurring e-waste contaminants (e.g., BDE-47, PCB118, PCB180, and PHE) did not significantly impair 6OCB degradation by consortium QZ3 (Fig. S3D–E), highlighting its environmental adaptability and potential for bioremediation in such settings. In addition, nutrient amendments (e.g., glucose and nitrogen sources) had negligible effects on CLCM biodegradation (Fig. S4), suggesting that the consortium maintained its intrinsic metabolic homeostasis during xenobiotic degradation.

Furthermore, a total of 19 potential transformation products of 6OCB were identified, with 14 and 5 classified as levels 3 and 4, respectively (Table S2, Fig. S5–S6), based on the metabolite annotation hierarchy proposed by Schymanski et al. (2014). Both Phase I reactions (hydrolysis, ether bond cleavage, reduction, oxidation, transamination, C–C bond breakage, and benzene ring opening) and Phase II conjugations (O-methylation, sulfonation, and glycosylation) were involved (Fig. 1D). Specifically, the cyano group of 6OCB first underwent sequential hydrolysis to form an amide intermediate (P298, $m/z = 298.1799$), which was further hydrolyzed to a carboxylic acid derivative (P299, $m/z = 299.1641$). A similar cyano group hydrolysis pathway has been reported in *Microvirga* sp. and *Lysobacter* sp. (Fu et al., 2024; Sun et al., 2024). The cyano group could also be reduced to an amino, generating P284 ($m/z = 284.2009$), which then underwent transamination to P283 ($m/z = 283.1696$) and subsequent oxidation to P299. Intermediate P299 was further transformed via three routes: (i) ether-bond cleavage to a biphenyl derivative ($m/z = 215.0703$), (ii) sulfonation to P393 ($m/z = 393.1012$), or (iii) O-glycosylation to P413 ($m/z = 459.2028$). Meanwhile, direct cleavage of the O-hexyl ether bond yielded P196 ($m/z = 196.0757$), which was hydrolyzed to P215. P196 was also reduced to P200 ($m/z = 200.1067$) and converted into P215 via transamination and oxidation. Ultimately, the ring-opening of P215 yielded P235 ($m/z = 235.0967$), which was further transformed into P181 ($m/z = 181.0495$) through hydroxylation-coupled oxidation. Notably, the C—C bond of the biphenyl skeleton in 6OCB was cleaved by concomitant hydroxylation, yielding the intermediates P120 ($m/z = 120.0444$) and P195 ($m/z = 195.1380$). P120 was then hydrolyzed to P137 ($m/z = 137.0245$), followed by O-methylation to yield P151 ($m/z = 151.0401$), whereas P195 produced hydroquinone (P109, $m/z = 109.0295$) via ether bond cleavage. These findings indicate that consortium QZ3 drives 6OCB biotransformation via diverse metabolic pathways. Notably, all tentatively identified degradation products, especially the downstream metabolites, exhibited lower predicted toxicity thresholds for aquatic organisms (fish, *daphnid*, and green algae) than the parent compound (Table S3 and S4). This observation suggests that consortium QZ3 mediates an enzymatic cascade that potentially detoxifies 6OCB during biodegradation. However, given that these products were identified at confidence levels 3–4, further structural confirmation and toxicological validation are required.

3.2. Characterization of consortium QZ3 via metagenomics and cultivation-dependent approaches

Metagenomic binning of > 205 Gbp clean data (192.49 Gbp from Illumina (Fig. S7A) and 12.72 Gbp from ONT sequencing) recovered 12 MAGs (Table S5). MAG1, classified as *Achromobacter* sp., dominated the consortium with an average relative abundance of 62.4 ± 3.6% (Fig. 2A), followed by MAG2 (*Ochrobactrum* sp., 22.2 ± 3.2%), MAG3 (*Shinella* sp., 11.2 ± 1.4%), MAG4 (*Sphingopyxis* sp., 1.2 ± 0.07%), MAG5 (*Alicycliphilus* sp., 1.5 ± 0.1%), and MAG6 (*Kaistella* sp., 1.2 ± 0.6%); the remaining MAGs each accounted for <1% relative abundance. This profile aligns with previous reports showing the prevalence of *Achromobacter* and *Ochrobactrum* in e-waste dismantling areas (Guo et al., 2021; Mu et al., 2018; Zhu et al., 2024), implying their adaptability to e-waste-derived contaminants.

To provide mechanistic insights into the integrated multi-omics analyses, eight pure strains were isolated from consortium QZ3 (Fig. S8 and S9, and Table S6). Four strains were identified at the species level (*Gordonia alkanivorans* QZP3, *Alicycliphilus denitrificans* QZW4, *Burkholderia contaminans* QZV1, and *Mycobacterium grossiae* QZY2) and four strains at the genus level (*Shinella* sp. QZW1, *Ochrobactrum* sp. QZW2, *Achromobacter* sp. QZW3, and *Mycobacterium* sp. QZY1). A phylogenetic tree incorporating MAGs, isolated strain genomes, and 70 reference genomes from the Genome Taxonomy Database (GTDB) revealed that *Shinella* sp. QZW1, *Ochrobactrum* sp. QZW2, *Achromobacter* sp. QZW3, *A. denitrificans* QZW4, and *Mycobacterium* sp. QZY1 were clustered with MAG7, MAG2, MAG1, MAG5, and MAG11, respectively (Fig. S10 and Fig. 2B). Given their superior genome quality relative to the corresponding MAGs, the isolated strain genomes were used as a reference set for downstream metatranscriptomic analysis. Notably, although metagenomic binning can recover broader genomic diversity, including uncultivated taxa, it often fails to capture extremely low-abundance members (Peng et al., 2025; Zhang et al., 2022a). For instance, short-read mapping indicated that *Gordonia* sp. was a rare taxon in the consortium, with an average relative abundance of only $(4.29 \pm 3.20) \times 10^{-5}$ (Fig. S7B), which is consistent with the established rarity thresholds (Wang et al., 2024b; Xue et al., 2018). Although no *Gordonia* MAG was recovered, *G. alkanivorans* QZP3 was successfully isolated. This highlighted the complementary value of combining metagenomics with cultivation to obtain a more complete genomic repertoire, which is essential for deciphering pollutant biodegradation mechanisms in acclimated microbial communities with large abundance disparities.

3.3. Roles of isolated strains in 6OCB biodegradation

Microcosm experiments were conducted to evaluate the 6OCB-degrading capabilities of the isolated strains under varying nutritional

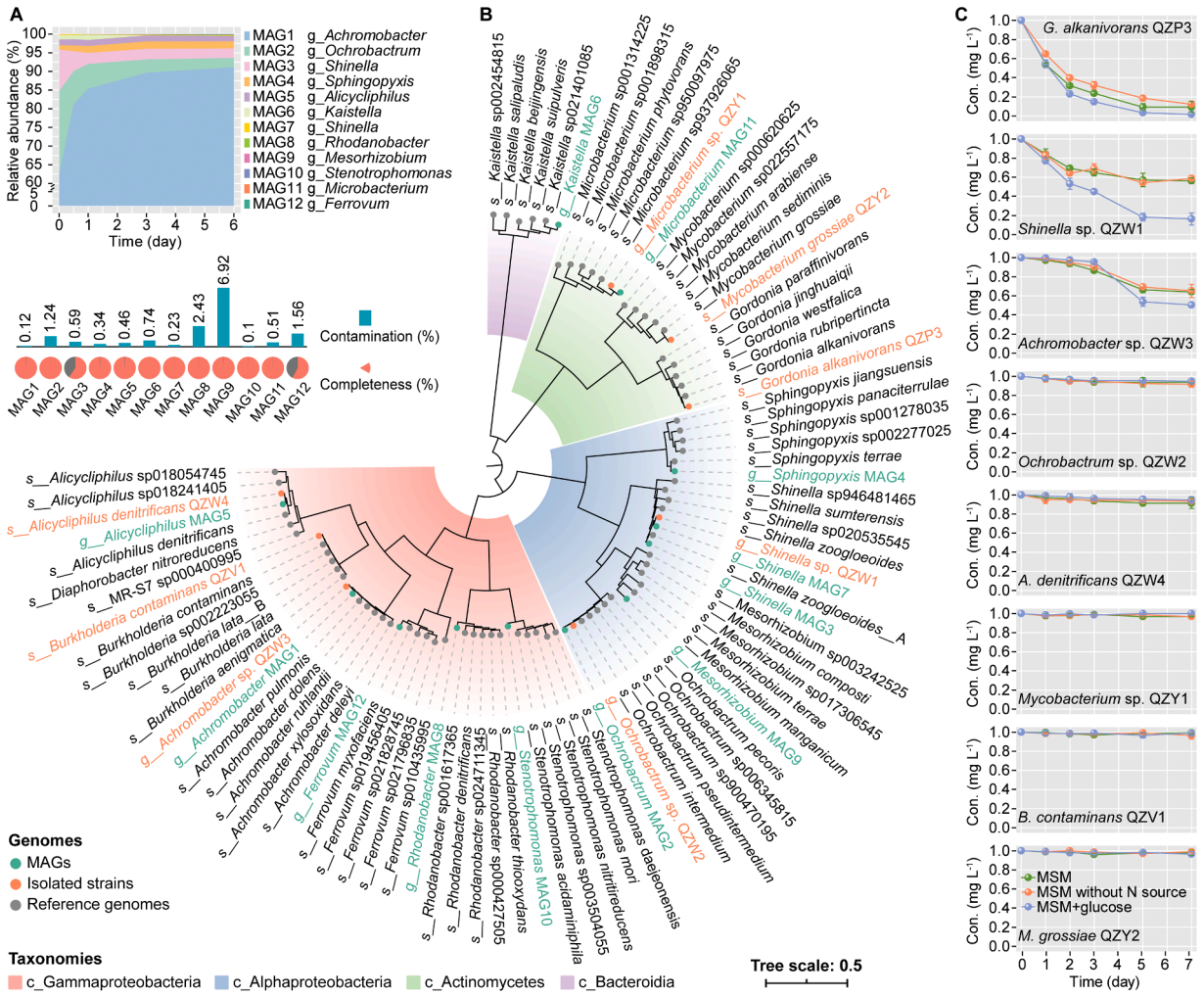

Fig. 2. Bacterial community profile of consortium QZ3. (A) Relative abundances and quality metrics (contamination and completeness) of 12 MAGs retrieved from metagenomic datasets, displayed as mean values of triplicates. (B) Phylogenetic tree of 12 MAGs and 8 isolated strain genomes compared with 70 reference genomes from the Genome Taxonomy Database (GTDB). (C) Degradation traits of 8 isolated strains toward 6OCB under different nutrient conditions. MSM stands for minimal salt medium. MSM + glucose represents adding 500 mg L^{-1} glucose to the medium. Data are shown as mean values ± SD (n = 3).

conditions. Strikingly, the low-abundance *G. alkanivorans* QZP3 exhibited high degradation efficiencies (90.6%–99.8%) regardless of the addition of exogenous glucose and/or nitrogen (Fig. 2C), which may underpin the excellent CLCM-degrading capacity observed at the community level. Previous studies have reported that rare taxa can drive core functions (e.g., xenobiotic degradation) in microbial communities (Peng et al., 2025; Zhao et al., 2025a). However, the actual quantitative contribution of *G. alkanivorans* QZP3 to community-level 6OCB degradation remains to be validated. Studies have also documented that *Gordonia* spp. are competent degraders of multiple recalcitrant compounds, including plasticizers (Wang et al., 2019), perfluorooctane sulfonate (Shaw et al., 2019), and plastics (Xu et al., 2025b). This study provides further evidence of LCM degradation by this genus, extending its documented bioremediation potential.

Shinella sp. QZW1 and *Achromobacter* sp. QZW3 also exhibited 6OCB-degrading activity, but their degradation efficiencies were markedly lower than that of *G. alkanivorans* QZP3 (Fig. 2C). Notably, glucose supplementation substantially enhanced their performance; for example, degradation by *Shinella* sp. QZW1 increased from 44.7% to 83.7% with 500 mg L^{-1} glucose, likely due to stimulated co-metabolism (Zhang et al., 2025a) and/or reduced cytotoxicity via promoted cell growth (Wu et al., 2024c). The observed cyanide degradation by *Shinella* sp. warrants further mechanistic investigation. Although *Achromobacter* spp. are recognized as dominant xenobiotic degraders in e-waste ecosystems (Guo et al., 2021; Zhu et al., 2024), *Achromobacter* sp. QZW3 showed limited 6OCB catabolic capability (Fig. 2C). Conversely, both *Ochrobactrum* sp. QZW2 and *A. denitrificans* QZW4 were identified as marginal 6OCB degraders, with degradation efficiencies below 8% regardless of nutritional supplementation. However, their higher relative abundances (MAG2 and MAG5) suggest that they may rely on 6OCB degradation products for growth. In addition, *Mycobacterium* sp. QZY1, *M. grossiae* QZY2, and *B. contaminans* QZV1 showed no detectable 6OCB degradation under any of the tested conditions (Fig. 2C), indicating that they may lack a competitive advantage in directly utilizing 6OCB within the community. To our knowledge, this is the first study to identify multiple CLCM-degrading bacterial strains, providing valuable microbial resources for the bioremediation of CLCM-contaminated hotspots.

3.4. Transcriptional profile of consortium QZ3 during 6OCB biodegradation

To elucidate the transcriptional dynamics of consortium QZ3 during 6OCB biodegradation, over 192 Gbp of metatranscriptomic datasets were generated from 15 samples. A time-series analysis identified 21,430 temporal tDEGs (Fig. S11), which were clustered into six distinct expression patterns (Fig. 3A). The KEGG annotation revealed that most tDEGs were associated with metabolism, biosynthesis, ABC transporters, two-component systems (TCSs), quorum sensing, and oxidative

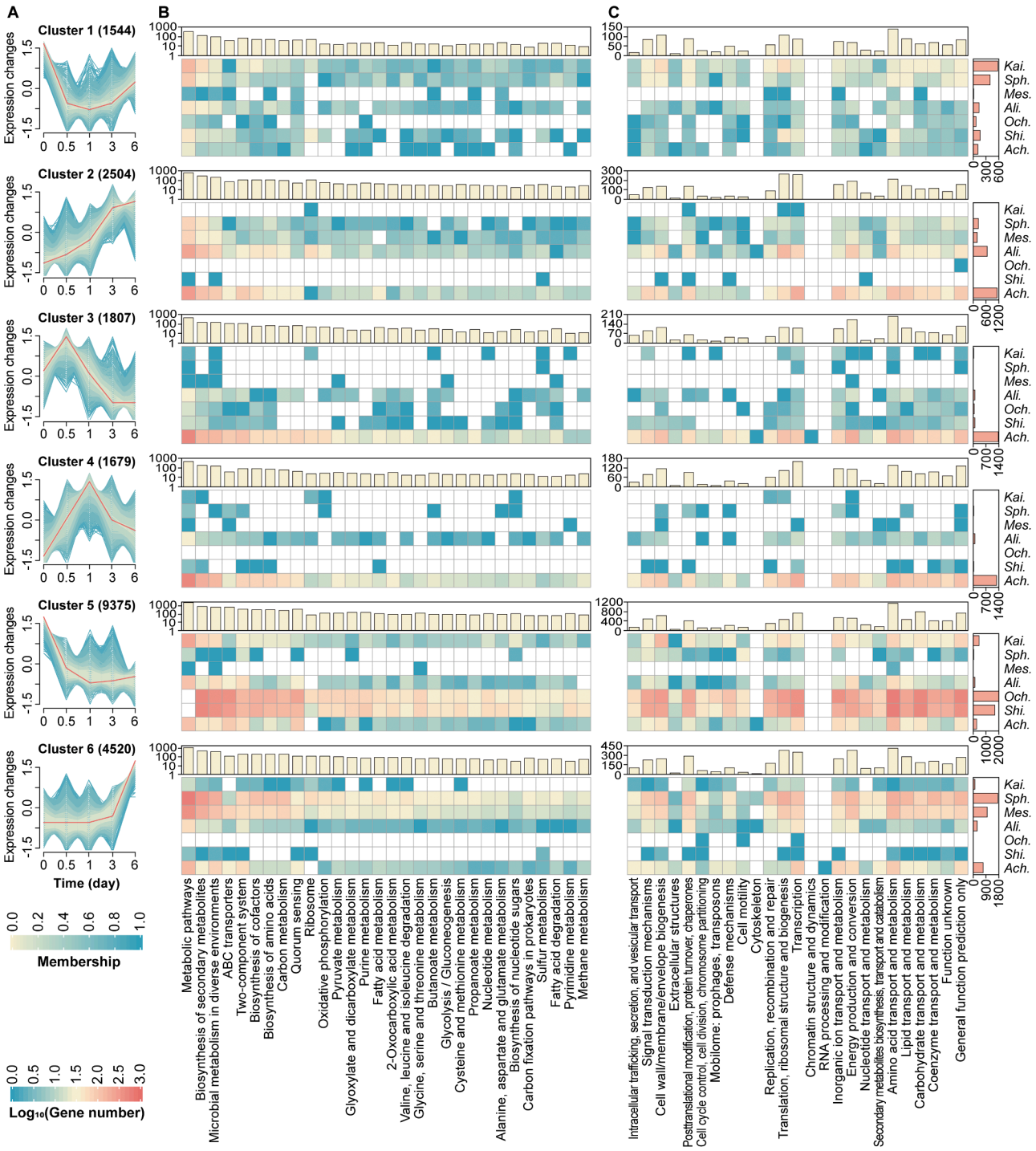

Fig. 3. Expression profiles and functional annotation of temporally differentially expressed genes (tDEGs) in consortium QZ3. (A) Dynamic expression profiles of tDEGs. Functional annotations of tDEGs in seven dominant species of consortium QZ3, including *Achromobacter* sp. (*Ach.*), *Shinella* sp. (*Shi.*), *Ochrobactrum* sp. (*Och.*), *Alicycliphilus* sp. (*Ali.*), *Mesorhizobium* sp. (*Mes.*), *Sphingopyxis* sp. (*Sph.*), and *Kaistella* sp. (*Kai.*), based on the Kyoto Encyclopedia of Genes and Genomes (KEGG) (B) and the Clusters of Orthologous Genes (COG) (C) databases. The top histograms show the total number of tDEGs in each functional category, while the right-side histograms show the total tDEG count for each strain.

phosphorylation across the seven dominant species (Fig. 3B). The COG analysis further confirmed the abundant tDEGs related to substrate transport and metabolism, transcription, and energy production and conversion (Fig. 3C), collectively underscoring their relevance to xenobiotic biodegradation.

The tDEGs in clusters 3 and 4, principally derived from *Achromobacter* sp., displayed an inverted U-shaped expression trajectory with marked upregulation within 0.5–1 day after inoculation, suggesting their involvement in initial adaptation and contaminant degradation. This pattern was consistent with the observed 6OCB degradation performance of *Achromobacter* sp. QZW3 (Fig. 2C). KEGG enrichment analysis confirmed significant enrichment of genes regulating oxidative phosphorylation, TCSs, bacterial secretion systems, and metabolism-related pathways (p-adjust < 0.05) (Fig. S12). Oxidative phosphorylation, the major ATP-yielding pathway in aerobes, may directly participate in xenobiotic degradation (Qiu et al., 2020). TCSs act as core

environmental-sensing mechanisms that regulate adaptive responses, including the induction of catabolic gene expression (Fu et al., 2023). For instance, multiple TCS-annotated genes in cluster 3, including *ccoP, ccoO, ccoQ, cydX*, and *cydB* (encoding cytochrome c/ubiquinol oxidase subunits), *pstS* (phosphate transport substrate-binding protein), *tctC* (tricarboxylic transport), *mexX* (multidrug efflux system component), and *fliC* (flagellin), were significantly upregulated during the early stages of 6OCB exposure (Table S7). These findings suggest that TCSs mediate a coordinated suite of adaptive responses during 6OCB degradation, encompassing redox and energy status sensing, responses to nutrient limitation, detoxification of toxic intermediates, and motility regulation. Similarly, bacterial secretion systems, which encode diverse transport proteins, likely mediate transmembrane transport of pollutants and efflux of intermediates (Meyer-Cifuentes et al., 2020). Cluster 2 tDEGs were persistently upregulated throughout degradation, especially on days 1–3 (Fig. 3A). Largely annotated to *Achromobacter* sp. and *Alicycliphilus* sp., they were significantly enriched in tricarboxylic acid cycle, biosynthesis of secondary metabolites and amino acids, and metabolic pathways (Fig. S12), highlighting their hosts' potential role in 6OCB metabolism. The tDEGs in clusters 1 and 6 were significantly upregulated during the late degradation phase, implying that their annotated members (e.g., *Sphingopyxis* sp., *Kaistella* sp., and *Mesorhizobium* sp.) may be involved in processing terminal degradation products. In contrast, tDEGs in cluster 5, primarily annotated as *Shinella* sp. and *Ochrobactrum* sp., were broadly downregulated within 24 h of 6OCB exposure (Fig. 3A), and were enriched for pathways governing bacterial chemotaxis, quorum sensing, and ABC transporters (Fig. S12). Early downregulation of chemotaxis- and quorum-sensing-related genes likely reflected an energy-conservation strategy, whereby motility suppression prioritizes metabolic adaptation over active locomotion (Tan et al., 2025; Zhang et al., 2022b).

3.5. Interspecies interactions and metabolic exchanges

Given that 6OCB served as the sole carbon and energy source, functional complementarity among community members likely facilitated cooperative catabolism. Pairwise co-cultures of the isolated strains revealed synergistic interactions across multiple strain pairs (Fig. 4). Notably, the co-culture of *G. alkanivorans* QZP3 with either *Shinella* sp. QZW1 or *M. grossiae* QZY2 significantly enhanced 6OCB degradation efficiency compared to the monoculture of *G. alkanivorans* QZP3 (Fig. 4A). This synergy likely contributed substantially to the outstanding 6OCB-degrading capacity of consortium QZ3. Although *M. grossiae* QZY2 did not degrade 6OCB, it exhibited marked synergistic effects when paired with *Shinella* sp. QZW1, *Achromobacter* sp. QZW3, *Ochrobactrum* sp. QZW2, or *B. contaminans* QZV1, increasing the degradation efficiency by 12.1%, 23.4%, 29.6%, and 53.4%, respectively (Fig. 4B–E). These results indicate that extensive interspecies interactions exist within this consortium and drive its core functional performance; such interactions occur not only between degraders and non-degraders, but also among non-degraders themselves. Notably, synergistic effects were observed when *Mycobacterium* sp. QZY1 was co-cultured with several strains (e.g., *Achromobacter* sp. QZW3, *B. contaminans* QZV1, and *Ochrobactrum* sp. QZW2) (Fig. 4C–E). These findings underscore the pivotal role of *Mycobacterium* spp. in underpinning efficient 6OCB biodegradation through interspecies cooperation. However, these assays used only a single 1:1 inoculum ratio; systematically optimizing strain ratios may further boost degradation by synergistic pairs and inform the design of high-performance synthetic consortia.

The GSMM analyses uncovered extensive metabolic interactions between the isolated strains and their non-redundant MAGs, with the exchanged metabolites primarily comprising homogeneous metal/non-metal compounds, organic acids and derivatives, organoheterocyclic

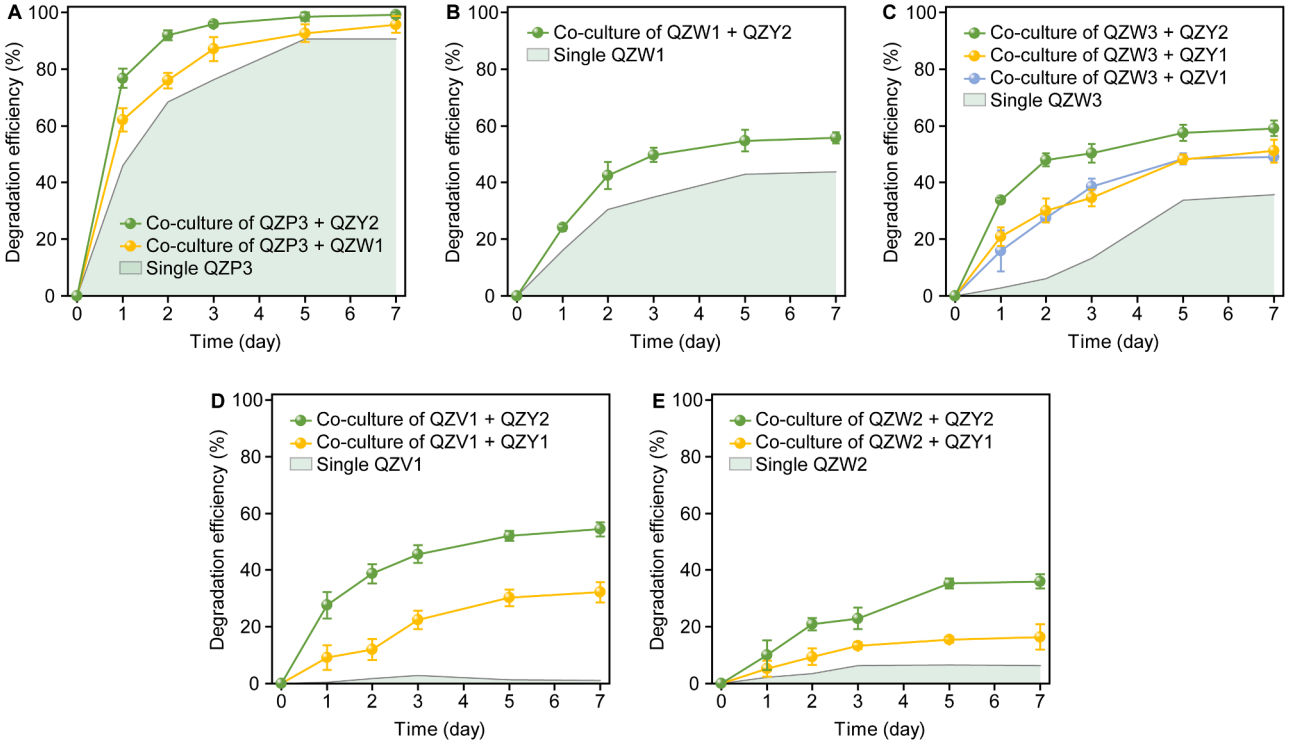

Fig. 4. Synergistic enhancement of 6OCB biodegradation by pairwise co-cultures of isolated strains. (A) *G. alkanivorans* QZP3 co-cultured with *Shinella* sp. QZW1 or *M. grossiae* QZY2; (B) *Shinella* sp. QZW1 co-cultured with *M. grossiae* QZY2; (C) *Achromobacter* sp. QZW3 co-cultured with *B. contaminans* QZV1, *Mycobacterium* sp. QZY1, or *M. grossiae* QZY2; (D) *B. contaminans* QZV1 co-cultured with *Mycobacterium* sp. QZY1 or *M. grossiae* QZY2; (E) *Ochrobactrum* sp. QZW2 co-cultured with *Mycobacterium* sp. QZY1, or *M. grossiae* QZY2. Data are shown as mean values ± SD (n = 3). Only co-cultures significantly outperforming their corresponding best-performing monoculture (shaded area) ($p < 0.05$, two-tailed Student's *t*-test, day 7) are shown.

compounds, and benzenoids (Fig. 5A and Fig. S13). As core 6OCB-degraders, most metabolites exchanged by *Shinella* sp. QZW1 (62.1%), *Achromobacter* sp. QZW3 (78.1%), and *G. alkanivorans* QZP3 (64.7%) were classified as outputs (Fig. 5B–E). For example, *Shinella* sp. QZW1 supplied diverse metabolites to *M. grossiae* QZY2 (e.g., L-alanine-D-glutamate-meso-2, and Fe^{3+}), *A. denitrificans* QZW4 (e.g., phosphate, and Fe^{3+}), MAG3 (e.g., ferrypyoverdine, inosine, and pyridoxine), MAG10 (e.g., ferrypyoverdine, and Fe^{2+} mitochondria), and MAG12 (e.g., L-valine, and Fe^{3+}) (Fig. 5C). *Achromobacter* sp. QZW3 exported metabolites to *M. grossiae* QZY2, MAG3, MAG4, MAG8, and MAG9, while also receiving multiple siderophores (e.g., Fe^{2+} mitochondria and Fe^{3+}) and glycerophosphoglycerol from *B. contaminans* QZV1, *Shinella* sp. QZW1, and *Ochrobactrum* sp. QZW2 (Fig. 5D), suggesting that it may benefit from such bidirectional metabolic cross-feeding to maintain its high relative abundance. Interestingly, *M. grossiae* QZY2 was found to participate extensively in metabolic exchange, acting as a donor to *Shinella* sp. QZW1, MAG3, MAG4, and MAG8, and as a recipient from *Shinella* sp. QZW1, *Achromobacter* sp. QZW3, *B. contaminans* QZV1, MAG3, and MAG9. This metabolic versatility may explain the enhanced 6OCB degradation observed in co-cultures with multiple partners.

Moreover, the rare taxon *G. alkanivorans* QZP3 engaged in extensive cross-feeding interactions with MAG3, MAG8, and MAG9, by supplying amino acids (e.g., L-arginine), siderophores (e.g., ferripyoverdine, Fe^{2+} mitochondria, and iron bound extracellular staphyloferrins), nucleic acid synthesis precursors (e.g., uracil and guanine), and nitrogen components (Fig. 5E). Siderophore-mediated cooperation is common in microbial interactions (Harrison et al., 2008). The non-degrader *Acinetobacter* sp. BD6 markedly enhanced dibenzo-p-dioxin degradation by supplying siderophores to the degrader *Rhodococcus* sp. p52 (Zhao et al., 2025b). Although rare taxa are often considered "cheaters" in microbial communities, their pivotal and multifaceted ecological roles are being increasingly recognized, including serving as genetic reservoirs that

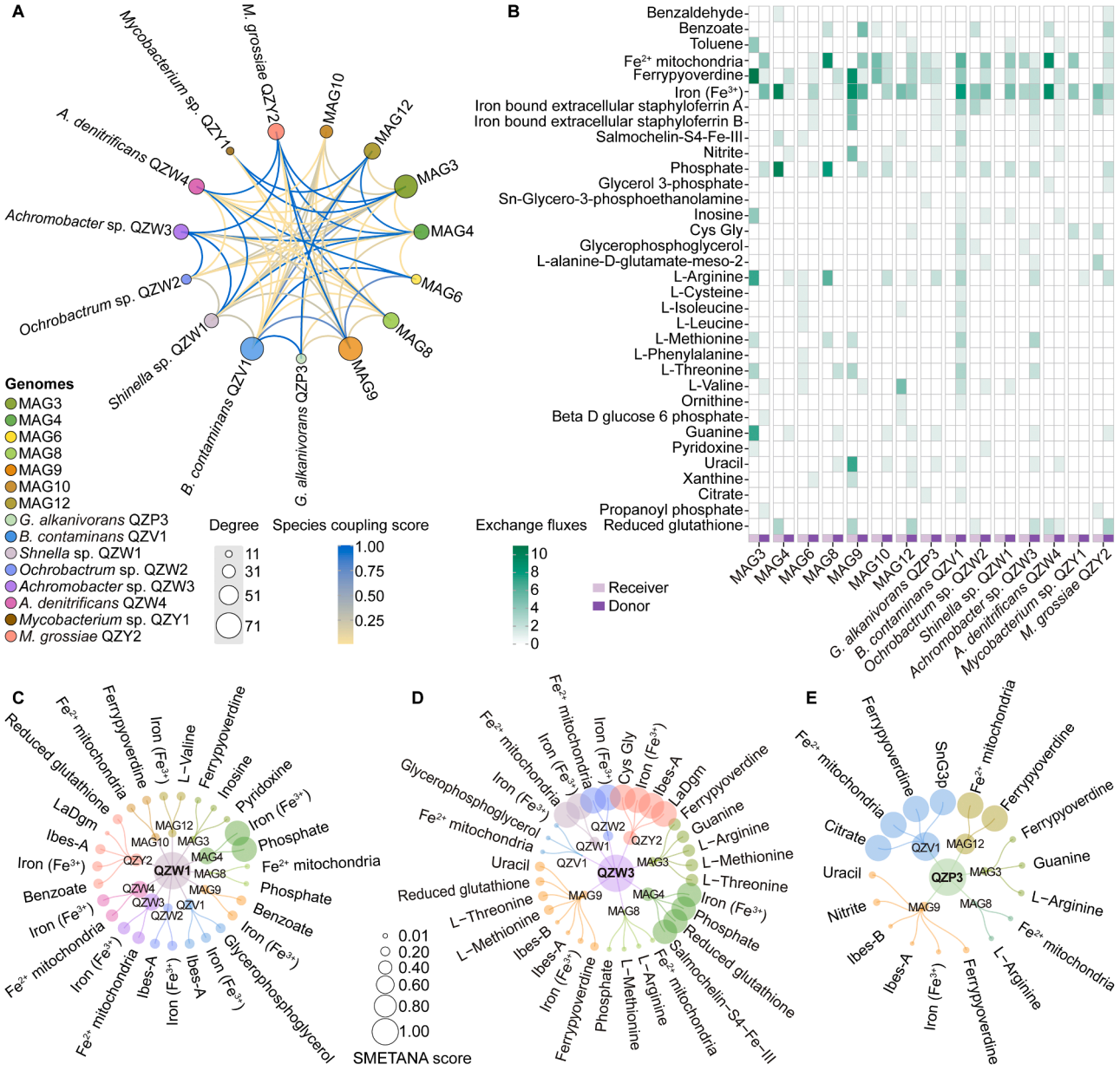

Fig. 5. Metabolic modeling of interspecies interactions in consortium QZ3. (A) Metabolic interactions among isolated strains and their non-redundant MAGs. (B) Metabolite exchange fluxes of each strain or MAG. Cross-feeding interactions between *Shinella* sp. QZW1 (C), *Achromobacter* sp. QZW3 (D), and *G. alkanivorans* QZP3 (E) with other members (Ibes-A: Iron bound extracellular staphyloferrin A, Ibes-B: Iron bound extracellular staphyloferrin B, LaDgm: L-alanine-D-glutamate-meso-2, SnG3p: Sn-Glycero-3-phosphoethanolamine).

underpin microbial community multifunctionality (Lennon and Jones, 2011), acting as primary degraders initiating polyhydroxybutyrate hydrolysis (Wang et al., 2026), and functioning as key drivers of nutrient acquisition (Dong et al., 2024). A recent study demonstrated that, in a coastal lignin-degrading consortium, rare species such as *Vibrio alginolyticus* and *S. putrefaciens* can promote the growth of the degrader *P. gergoviae* and enhance lignin degradation by sharing amino acids and alcohols (Peng et al., 2025). Herein, our results further suggest that the rare species *G. alkanivorans* QZP3 likely drives the key functionality of consortium QZ3 and may support non-degraders via metabolic cross-feeding. It should be noted that these *in silico* metabolic cross-feeding predictions from GSMMs require further experimental validation. In addition, the present study only tested pairwise interactions. It is of great importance to further validate the degradation potential and ecological effects of multi-strain synthetic consortia (e.g., *Achromobacter* sp. QZW3, *M. grossiae* QZY2, and *B. contaminans* QZV1, which were predicted by GSMMs to exhibit extensive pairwise metabolic cross-feeding) for in situ remediation.

3.6. Metabolic mechanisms of 6OCB by key members of consortium QZ3

Given the pivotal role of *G. alkanivorans* QZP3 in 6OCB degradation and the infeasibility of genome assembly owing to its extremely low abundance in consortium QZ3, comparative proteomic analyses were conducted to elucidate the underlying metabolic mechanisms. A total of 604 DEPs were identified in response to 6OCB exposure, comprising 211 upregulated and 393 downregulated proteins (Fig. S14A–B). Functional enrichment analysis revealed that these DEPs were primarily enriched in GO terms including cellular anatomical entity, membrane, and cation binding, as well as KEGG pathways including ABC transporters, TCS, pyruvate metabolism, and benzoate degradation (Fig. S14C–D). Specifically, exposure to 6OCB induced a 2.35-fold upregulation of apolipoprotein N-acyltransferase (W9DJF5). This protein belongs to the COG0388 superfamily, which includes nitrilase, cyanide hydratase, and related acyltransferase homologs. Its conserved PF00795.26 domains (characteristic of the carbon-nitrogen hydrolase family) further support its potential to cleave cyanide-related C—N bonds. Molecular docking analyses revealed a favorable binding configuration between 6OCB and W9DJF5, with a binding energy of −6.93 kcal/mol stabilized by conventional hydrogen bonds, alkyl, π-alkyl, and π-anion interactions (Fig. 6A). These findings suggest that W9DJF5 may contribute to the initial hydrolysis of the cyano group in 6OCB. Similarly, thiocyanate hydrolase subunit gamma (W9DI63), a protein previously reported to mediate cyano group hydrolysis in *Thiobacillus* sp. (Arakawa et al., 2007), showed a binding energy of −7.24 kcal/mol for 6OCB. This protein-ligand interaction was stabilized by a hydrogen bond formed between the guanidino group of Arg212 and the cyano nitrogen atom of the 6OCB ligand (Fig. 6B). The hydrolysis of the cyano group to a

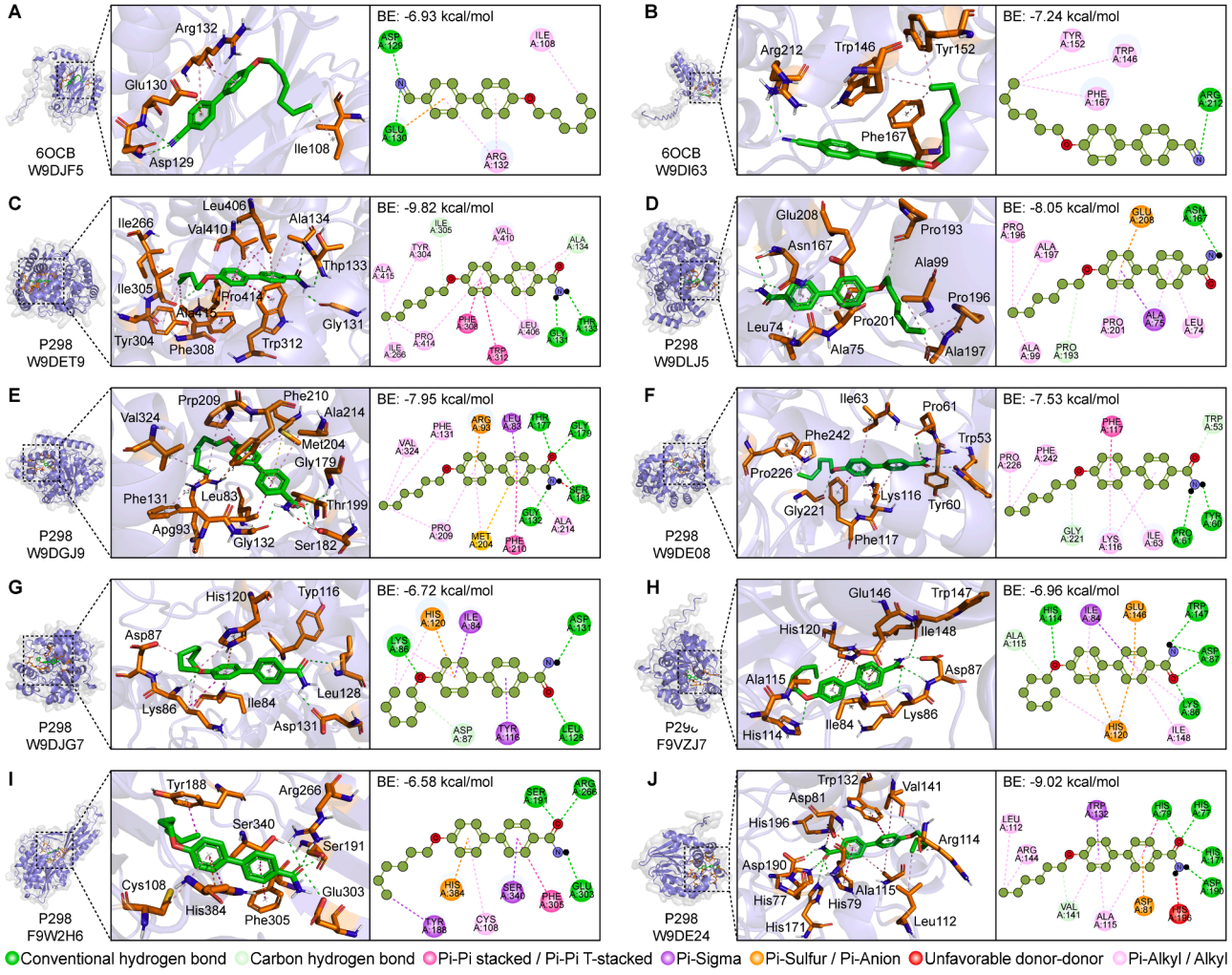

Fig. 6. Molecular binding interactions of 6OCB and its amide intermediate (P298) with key functional enzymes. Apolipoprotein N-acyltransferase (W9DJF5), thiocyanate hydrolase subunit gamma (W9DI63), amidase (W9DET9, W9DLJ5, and W9DGJ9), amidohydrolase (W9DE08, and W9DJG7), putative amidohydrolase (F9VZJ7, and F9W2H6), and beta-lactamase (W9DE24).

carboxyl group, a key step in cyanide degradation, was further supported by the significant upregulation of amide-hydrolyzing enzymes, including amidase (e.g., W9DET9, W9DLJ5, W9DGJ9), amidohydrolase (W9DE08, W9DJG7), putative amidohydrolase (F9VZJ7, F9W2H6), and beta-lactamase (W9DE24) (Fig. 6C–J), all of which are known to cleave amide bonds (Fu et al., 2024; Jiang et al., 2023). Although nitrile reductases typically catalyze the NAD(P)H-dependent reduction of the cyano group to primary amines (-CH_2NH_2) (Ribeiro et al., 2015; Zhou et al., 2018), no dedicated nitrile reductase was identified in *G. alkanivorans* QZP3, suggesting that alternative oxidoreductases may mediate this reductive transformation. Two aminotransferases (F9W1Z6 and W9DA20), which showed favorable binding to the amino-containing intermediates P284 and P200 (Fig. S15A–D), likely catalyze the conversion of these intermediates to the corresponding aldehyde products P283 and P199. These aldehydes are subsequently oxidized to carboxylic acid metabolites (P299 and P215) by aldehyde dehydrogenase (W9DEA2) (Fig. S15E–F). Together, these results elucidate the molecular mechanism by which *G. alkanivorans* QZP3 initiates transformation of the cyanide moiety of 6OCB.

Furthermore, a cytochrome P450 (B3IX64) and a putative cytochrome P450 (F9VRL8) were upregulated 1.30- and 2.47-fold, respectively, and exhibited binding energies of −8.32 and −8.21 kcal/mol with 6OCB (Fig. S15G–H). Given their reported roles in ether bond cleavage and hydroxylation during xenobiotic biodegradation (Malandain et al., 2010), these enzymes are proposed to mediate the oxidative cleavage of the hexoxy-ether linkage in 6OCB, yielding P196 and aliphatic alcohols. A putative aromatic hydrocarbon dioxygenase small subunit (F9VSN2), which was upregulated 1.74-fold and showed a binding energy of −6.31 kcal/mol, may participate in hydroxylative cleavage of the biphenyl skeleton (Fig. S15I). This catalytic mechanism is analogous to that reported for *Gordonia* sp. PS3 in the biodegradative cleavage of polystyrene (Xu et al., 2025b). Three sulfonation-related enzymes [sulfotransferases (F9VUM8 and F9VYT3) and a sulfotransferase family protein (F9VX80)] and two glycosylation-related proteins [peptidoglycan glycosyltransferase (F9VWA3) and malto-oligosyltrehalose synthase (F9VY60)] exhibited stable binding to intermediate P299 (Fig. S16), suggesting that they are involved in Phase II metabolism via sulfonation and glycosylation. Therefore, the enzymes identified in this study represent high-priority candidates for further functional validation through heterologous expression and in vitro enzymatic activity assays.

The reconstruction of key metabolic pathways based on KEGG annotation revealed that *G. alkanivorans* QZP3 encodes a nearly complete benzoate degradation pathway (Fig. S17), indicating its capacity to metabolize benzoate-derived intermediates such as P137 and P151. The presence of complete fatty acid biosynthesis and degradation pathways suggests that hexoxy-derived aliphatic metabolites can be catabolized to acetyl-CoA via β-oxidation, which highlights the strain's metabolic versatility in catabolizing CLCM alkyl chains. Moreover, functional pathways associated with carbon fixation, nitrogen and sulfur metabolisms were identified, indicating that the degradation intermediates are efficiently incorporated into the central metabolism to support biomass synthesis and maintain redox homeostasis during 6OCB biodegradation. These findings indicate that *G. alkanivorans* QZP3 orchestrates a network of xenobiotic and primary metabolic pathways that potentially enables 6OCB detoxification and supports metabolic complementarity with other consortium members.

In addition, we discussed the potential genes and enzymes involved in 6OCB degradation by *Shinella* sp. QZW1 and *Achromobacter* sp. QZW3 based on the mapping of metatranscriptomic reads to their respective reference genomes, as detailed in Text S8. The results revealed that *Achromobacter* sp. QZW3 primarily utilizes an upregulated nitrilase for initial cyano group hydrolysis, while *Shinella* sp. QZW1 relies on nitrile hydratase subunits. Both strains also harbor significantly induced genes encoding amidohydrolases, aminotransferases, and ether bond-cleaving enzymes, which may mediate the downstream multi-pathway transformation of 6OCB. Taken together, this integrated multi-omics analysis demonstrated that the core microbial members of consortium QZ3 harbor relatively complete and complementary metabolic pathways for the biodegradation of this representative CLCM.

4. Conclusions

In this study, we established a CLCM-degrading consortium (QZ3) via a "top-down" targeted enrichment strategy. This consortium exhibited marked structure-dependent specificity in the degradation of representative CLCMs, with alkyl chain length identified as a key factor governing their biodegradability. We pinpointed the core functional degraders within the consortium, including *G. alkanivorans* QZP3, *Shinella* sp. QZW1, and *Achromobacter* sp. QZW3. Notably, the low-abundance *G. alkanivorans* QZP3 exhibited superior CLCM degradation capability, and harbored genetic and enzymatic versatility to mediate multi-pathway CLCM biotransformation. This finding emphasizes that understudied rare taxa could serve as keystone drivers contributing to community-level xenobiotic degradation, highlighting the ecological importance of the rare biosphere. We further uncovered widespread synergistic interactions among the isolated strains that markedly boosted CLCM biodegradation efficiency. Critically, these synergistic effects were not limited to interactions between degraders and non-degraders, but also occurred among non-degraders themselves. Particularly, two *Mycobacterium* sp. established cooperative networks with multiple partners through metabolite cross-feeding (mainly involving amino acids, siderophores, and nucleic acid precursors), suggesting that non-degrading commensal strains may contribute to promoting and stabilizing community-level degradation functions. However, future studies are warranted to verify the functional roles of low-abundance degraders via targeted approaches (e.g., DNA-stable isotope probing, Raman-activated single-cell sorting) and to quantitatively dissect the metabolic cross-feeding mechanism through constructing simplified synthetic consortia. Overall, this study deciphers the underlying molecular and ecological mechanisms of typical CLCM degradation by complex microbial consortia, and provides a mechanistic framework for the rational design of high-performance synthetic microbial consortia, thereby informing future strategies for engineered bioremediation and sustainable e-waste management.

CRediT authorship contribution statement

Minghan Zhu: Writing – review & editing, Writing – original draft, Visualization, Validation, Methodology, Investigation, Funding acquisition, Formal analysis, Data curation, Conceptualization. **Chang He:** Writing – review & editing, Writing – original draft, Resources, Investigation, Formal analysis. **Shaoyu Tang:** Writing – review & editing, Writing – original draft, Supervision, Resources, Project administration, Funding acquisition, Conceptualization. **Jiayu Zhang:** Writing – review & editing, Writing – original draft, Methodology, Formal analysis. **Zhen Yu:** Writing – review & editing, Writing – original draft, Resources, Methodology. **Hui Lin:** Writing – review & editing, Writing – original draft, Resources, Methodology. **Yibo Yuan:** Writing – review & editing, Writing – original draft, Visualization, Investigation, Formal analysis. **Jonathan W.C. Wong:** Writing – review & editing, Writing – original draft, Resources. **Hua Yin:** Writing – review & editing, Writing – original draft, Supervision, Resources, Conceptualization. **Junfeng Niu:** Writing – review & editing, Writing – original draft, Resources. **Xujun Liang:** Writing – review & editing, Writing – original draft, Resources. **Zhi Dang:** Writing – review & editing, Writing – original draft, Supervision, Resources, Project administration.

Declaration of competing interest

The authors declare that they have no known competing financial interests or personal relationships that could have appeared to influence

the work reported in this paper.

Acknowledgements

This work was jointly supported by the National Natural Science Foundations of China (42407301 and 42577317), Guangdong Basic and Applied Basic Research Foundation (2023A1515110024), and the Key Laboratory of Pollution Control and Ecosystem Restoration in Industry Clusters, Ministry of Education.

Supplementary materials

Supplementary material associated with this article can be found, in the online version, at doi:10.1016/j.watres.2026.126259.

Data availability

Data will be made available on request.

References

Anders, S., Pyl, P.T., Huber, W., 2015. HTSeq–a Python framework to work with high-throughput sequencing data. Bioinformatics 31 (2), 166–169. https://doi.org/10.1093/bioinformatics/btu638.

Arakawa, T., Kawano, Y., Kataoka, S., Katayama, Y., Kamiya, N., Yohda, M., Odaka, M., 2007. Structure of thiocyanate hydrolase: a new nitrile hydratase family protein with a novel five-coordinate cobalt(iii) center. J. Mol. Biol. 366 (5), 1497–1509. https://doi.org/10.1016/j.jmb.2006.12.011.

Balde, C.P., Kuehr, R., Yamamoto, T., McDonald, R., D'Angelo, E., Althaf, S., Bel, G., Deubzer, O., Fernandez-Cubillo, E., Forti, V., Gray, V., Herat, S., Honda, S., Iattoni, G., Khetriwal, D.S., Luda di Cortemiglia, V., Lobuntsova, Y., Nnorom, I., Pralat, N., Wagner, M., 2024. The Global E-Waste Monitor 2024. International Telecommunication Union (ITU) and United Nations Institute for Training and Research (UNITAR).. https://ewastemonitor.info/the-global-e-waste-monitor-2024/

Chen, S., Zhou, Y., Chen, Y., Gu, J., 2018. Fastp: an ultra-fast all-in-one FASTQ preprocessor. Bioinformatics 34 (17), i884–i890. https://doi.org/10.1093/bioinformatics/bty560.

Dong, X., Chen, M., Chen, Q., Liu, K., Long, J., Li, Y., Ren, Y., Yang, T., Zhou, J., Herath, S., Peng, X., 2024. Rare microbial taxa as the major drivers of nutrient acquisition under moss biocrusts in karst area. Front. Microbiol. 15, 1384367. https://doi.org/10.3389/fmicb.2024.1384367.

Duan, L., Liang, J., Zhang, W., Liu, Z., Kang, H., Huang, D., Wang, Z., Jiang, G., Gao, A., 2025. The liquid crystal monomer EtCBN induced neurotoxicity by activating the NOD-like receptor signaling pathway through the muribaculum-epigallocatechin axis. J. Hazard. Mater. 496, 139206. https://doi.org/10.1016/j.jhazmat.2025.139206.

Ecological Structure-Activity Relationships (ECOSAR) Predictive Model, 2023. Version 2.2. U.S. environmental protection agency, W., DC. https://www.epa.gov/tsca-screening-tools/ecological-structure-activity-relationships-ecosar-predictive-model.

El-Hachem, N., Haibe-Kains, B., Khalil, A., Kobeissy, F.H., Nemer, G., 2017. In: Kobeissy, F.H., Stevens, J.S.M. (Eds.), Neuroproteomics: Methods and Protocols. Springer New York, New York, NY, pp. 391–403. Eds.

Feng, Y., Wu, J., Lao, W., Ye, W., Guo, D., Wang, Z., Wu, X., Lai, R.W.S., 2025. Micro- and nanoplastic-mediated phototransformation and bioaccessibility of fluorinated liquid crystal monomer in aquatic environments. Environ. Sci.: Nano 12 (1), 248–261. https://doi.org/10.1039/D4EN00723A.

Fu, Q., Hu, T., Yang, Y., Zhao, M., 2023. Transcriptome analysis reveals phenanthrene degradation strategy of *Pseudomonas stutzeri* LH-42. 3 Biotech 13 (2), 1–12. https://doi.org/10.1007/s13205-023-03473-7.

Fu, X., Fei, Q., Zhang, X., Li, N., Zhang, L., Zhou, Y., 2024. Two different types of hydrolases co-degrade ochratoxin A in a highly efficient degradation strain *lysobacter* sp. CW239. J. Hazard. Mater. 473, 134716. https://doi.org/10.1016/j.jhazmat.2024.134716.

Giordano, N., Gaudin, M., Trottier, C., Delage, E., Nef, C., Bowler, C., Chaffron, S., 2024. Genome-scale community modelling reveals conserved metabolic cross-feedings in epipelagic bacterioplankton communities. Nat. Commun. 15, 2721. https://doi.org/10.1038/s41467-024-46374-w.

Guo, Z., Yin, H., Wei, X., Zhu, M., Lu, G., Dang, Z., 2021. Effects of methanol on the performance of a novel BDE-47 degrading bacterial consortium QY2 in the co-metabolism process. J. Hazard. Mater. 415, 125698. https://doi.org/10.1016/j.jhazmat.2021.125698.

Harrison, F., Paul, J., Massey, R.C., Buckling, A., 2008. Interspecific competition and siderophore-mediated cooperation in *Pseudomonas aeruginosa*. ISME J. 2 (1), 49–55. https://doi.org/10.1038/ismej.2007.96.

He, S., Shen, M., Wu, E., Yin, R., Zhu, M., Zeng, L., 2022. Molecular structure on the detoxification of fluorinated liquid crystal monomers with reactive oxidation species in the photocatalytic process. Environ. Sci. Ecotechnol. 9, 100141. https://doi.org/10.1016/j.ese.2021.100141.

Jiang, H., Li, H., Wang, Y., Yu, X., Chen, X., Dai, Y., 2023. Biodegradation of the nitrile-containing insecticides sulfoxaflor, flonicamid, thiacloprid, and acetamiprid by immobilized *Escherichia coli* harboring genes of nitrile hydratase and a cobalt transporter. J. Environ. Chem. Eng. 11 (2), 109521. https://doi.org/10.1016/j.jece.2023.109521.

Jiang, Y., Zeng, Y., Long, L., Guo, J., Lu, R., Chen, P., Pan, Z., Zhang, Y., Luo, X., Mai, B., 2024. First report on the trophic transfer and priority list of liquid crystal monomers in the pearl river estuary. Environ. Sci. Technol. 58 (36), 16131–16141. https://doi.org/10.1021/acs.est.4c04962.

Kong, Y., Yang, X., Zhou, S., Zhou, P., Juhasz, A., Su, G., Zhang, Q., Cui, X., 2025. In vivo bioavailability of liquid crystal monomers (LCMs) in indoor dust: implications for human oral exposure. Environ. Sci. Technol. 59 (27), 13683–13692. https://doi.org/10.1021/acs.est.5c04078.

Kopylova, E., Noé, L., Touzet, H., 2012. SortMeRNA: fast and accurate filtering of ribosomal RNAs in metatranscriptomic data. Bioinformatics 28 (24), 3211–3217. https://doi.org/10.1093/bioinformatics/bts611.

Kost, C., Patil, K.R., Friedman, J., Garcia, S.L., Ralser, M., 2023. Metabolic exchanges are ubiquitous in natural microbial communities. Nat. Microbiol. 8 (12), 2244–2252. https://doi.org/10.1038/s41564-023-01511-x.

Langmead, B., Salzberg, S.L., 2012. Fast gapped-read alignment with Bowtie 2. Nat. Methods 9 (4), 357–359. https://doi.org/10.1038/nmeth.1923.

Lennon, J.T., Jones, S.E., 2011. Microbial seed banks: the ecological and evolutionary implications of dormancy. Nat. Rev. Microbiol. 9 (2), 119–130. https://doi.org/10.1038/nrmicro2504.

Li, R., Ren, K., Su, H., Wei, Y., Su, G., 2023. Target and suspect analysis of liquid crystal monomers in soil from different urban functional zones. Sci. Total Environ. 854, 158408. https://doi.org/10.1016/j.scitotenv.2022.158408.

Liu, L., Tian, C., Wang, M., Luo, Y., Huang, Y., Jiang, T., Zhao, H., Yu, Q., Wang, E., Yang, J., Yuan, H., 2025. Mutualism between degraders and nondegraders stabilizes the function of a natural biopolymer-degrading community. Proc. Natl. Acad. Sci. 122 (30), e2500664122. https://doi.org/10.1073/pnas.2500664122.

Liu, Q., Liggio, J., Wentzell, J., Lee, P., Li, K., Li, S.-M., 2020. Atmospheric OH oxidation chemistry of particulate liquid crystal monomers: an emerging persistent organic pollutant in air. Environ. Sci. Technol. Lett. 7 (9), 646–652. https://doi.org/10.1021/acs.estlett.0c00447.

Liu, Y., Li, W.-L., Li, Z.-M., Kannan, K., 2024. A method for the determination of 60 liquid crystal monomers in biotic and abiotic samples. Environ. Chem. Ecotoxicol. 6, 51–64. https://doi.org/10.1016/j.enceco.2024.01.003.

Lokesh, K., Matthias, E.F., 2007. Mfuzz: a software package for soft clustering of microarray data. Bioinformation 2 (1), 5–7. https://doi.org/10.6026/97320630002005.

Love, M.I., Huber, W., Anders, S., 2014. Moderated estimation of fold change and dispersion for RNA-seq data with DESeq2. Genome Biol. 15 (12), 550. https://doi.org/10.1186/s13059-014-0550-8.

Ma, X., Liang, B., Qi, M., Yun, H., Shi, K., Li, Z., Guo, Y., Yan, P., Liu, S.J., Wang, A., 2020. Novel pathway for chloramphenicol catabolism in the activated sludge bacterial isolate *sphingobium* sp. CAP-1. Environ. Sci. Technol. 54 (12), 7591–7600. https://doi.org/10.1021/acs.est.9b07324.

Machado, D., Andrejev, S., Tramontano, M., Patil, K.R., 2018. Fast automated reconstruction of genome-scale metabolic models for microbial species and communities. Nucleic Acids Res. 46 (15), 7542–7553. https://doi.org/10.1093/nar/gky537.

Malandain, C., Fayolle-Guichard, F., Vogel, T.M., 2010. Cytochromes P450-mediated degradation of fuel oxygenates by environmental isolates. FEMS Microbiol. Ecol. 72 (2), 289–296. https://doi.org/10.1111/j.1574-6941.2010.00847.x.

Meyer-Cifuentes, I.E., Werner, J., Jehmlich, N., Will, S.E., Neumann-Schaal, M., Ozturk, B., 2020. Synergistic biodegradation of aromatic-aliphatic copolyester plastic by a marine microbial consortium. Nat. Commun. 11, 5790. https://doi.org/10.1038/s41467-020-19583-2.

Mu, Y., Jia, W., Ke, Z., Zhuang, W., Wang, H., Jiang, J., Chen, K., Chen, Q., 2018. *Shinella pollutisoli* sp. nov., isolated from tetrabromobisphenol A-contaminated soil. Int. J. Syst. Evol. Microbiol. 68 (8), 2602–2606. https://doi.org/10.1099/ijsem.0.002883.

O'Boyle, N.M., Banck, M., James, C.A., Morley, C., Vandermeersch, T., Hutchison, G.R., 2011. Open Babel: an open chemical toolbox. J. Cheminform. 3, 33. https://doi.org/10.1186/1758-2946-3-33.

Peng, Q., Zhao, C., Wang, X., Cheng, K., Wang, C., Xu, X., Lin, L., 2025. Modeling bacterial interactions uncovers the importance of outliers in the coastal lignin-degrading consortium. Nat. Commun. 16, 639. https://doi.org/10.1038/s41467-025-56012-8.

Qi, X., Zhu, M., Yuan, Y., Rong, X., Dang, Z., Yin, H., 2023. Integrated toxicology, metabolomics, and transcriptomics analyses reveal the biodegradation and adaptation mechanisms to BDE-47 in *Pseudomonas plecoglossicida*. Chem. Eng. J. 454, 140412. https://doi.org/10.1016/j.cej.2022.140412.

Qiu, L., Fang, W., He, H., Liang, Z., Zhan, Y., Lu, Q., Liang, D., He, Z., Mai, B., Wang, S., 2020. Organohalide-respiring bacteria in polluted urban rivers employ novel bifunctional reductive dehalogenases to dechlorinate polychlorinated biphenyls and tetrachloroethene. Environ. Sci. Technol. 54 (14), 8791–8800. https://doi.org/10.1021/acs.est.0c01569.

Ribeiro, A.J.M., Yang, L., Ramos, M.J., Fernandes, P.A., Liang, Z.-X., Hirao, H., 2015. Insight into enzymatic nitrile reduction: QM/MM study of the catalytic mechanism of QueF nitrile reductase. ACS Catal. 5 (6), 3740–3751. https://doi.org/10.1021/acscatal.5b00528.

Ruan, Z., Tan, J., Feng, Q., Yang, K., Li, D., Chao, Y., Wang, P., Ni, Z., Chen, J., Qiu, R., 2025. Potentiators empower synthetic microbiomes as silent guardians against co-contamination. Nat. Commun. 17, 1185. https://doi.org/10.1038/s41467-025-67953-5.

Schwengers, O., Jelonek, L., Dieckmann, M.A., Beyvers, S., Blom, J., Goesmann, A., 2021. Bakta: rapid and standardized annotation of bacterial genomes via alignment-

free sequence identification. Microb. Genom. 7 (11), 000685. https://doi.org/10.1099/mgen.0.000685.
Schymanski, E.L., Jeon, J., Gulde, R., Fenner, K., Ruff, M., Singer, H.P., Hollender, J., 2014. Identifying small molecules via high resolution mass spectrometry: communicating confidence. Environ. Sci. Technol. 48 (4), 2097–2098. https://doi.org/10.1021/es5002105.
Sereika, M., Mussig, A.J., Jiang, C., Knudsen, K.S., Jensen, T.B.N., Petriglieri, F., Yang, Y., Jørgensen, V.R., Delogu, F., Sørensen, E.A., Nielsen, P.H., Singleton, C.M., Hugenholtz, P., Albertsen, M., 2025. Genome-resolved long-read sequencing expands known microbial diversity across terrestrial habitats. Nat. Microbiol. 10 (8), 2018–2030. https://doi.org/10.1038/s41564-025-02062-z.
Shaw, D.M.J., Munoz, G., Bottos, E.M., Duy, S.V., Sauvé, S., Liu, J., Van Hamme, J.D., 2019. Degradation and defluorination of 6:2 fluorotelomer sulfonamidoalkyl betaine and 6:2 fluorotelomer sulfonate by *gordonia* sp. strain NB4-1Y under sulfur-limiting conditions. Sci. Total Environ. 647, 690–698. https://doi.org/10.1016/j.scitotenv.2018.08.012.
Shen, M., Feng, Z., Liang, X., Chen, H., Zhu, C., Du, B., Li, Q., Zeng, L., 2022. Release and gas–particle partitioning behavior of liquid crystal monomers during the dismantling of waste liquid crystal display panels in e-waste recycling facilities. Environ. Sci. Technol. 56 (5), 3106–3116. https://doi.org/10.1021/acs.est.1c07394.
Su, H., Shi, S., Zhu, M., Crump, D., Letcher, R.J., Giesy, J.P., Su, G., 2019. Persistent, bioaccumulative, and toxic properties of liquid crystal monomers and their detection in indoor residential dust. Proc. Natl. Acad. Sci 116 (52), 26450–26458. https://doi.org/10.1073/pnas.1915322116.
Sun, S., Guo, J., Zhu, Z., Zhou, J., 2024. Microbial degradation mechanisms of the neonicotinoids acetamiprid and flonicamid and the associated toxicity assessments. Front. Microbiol. 15, 1500401. https://doi.org/10.3389/fmicb.2024.1500401.
Tan, X., Wang, R., Al-Dhabi, N.A., Wang, B., Chen, R., Zhang, Q., Zhou, D., Tang, W., Wang, H., 2025. Exploring the regulation mechanism of signaling molecules on algal-bacterial granular sludge through different N-acyl-homoserine lactones. Chin. Chem. Lett. 36 (7), 110515. https://doi.org/10.1016/j.cclet.2024.110515.
Wang, B., Zhang, Y., Wang, X., Hou, J., Zhao, K., Liu, W., 2026. Environmental drivers and microbial community dynamics underlying polyhydroxybutyrate (PHB) biodegradation in soil: the critical role of rare taxa. Water Air Soil Pollut. 237 (13), 743. https://doi.org/10.1007/s11270-026-09433-0.
Wang, Y., Jin, Q., Lin, H., Xu, X., Leung, K.M.Y., Kannan, K., He, Y., 2024a. A review of liquid crystal monomers (LCMs) as emerging contaminants: environmental occurrences, emissions, exposure routes and toxicity. J. Hazard. Mater. 480, 135894. https://doi.org/10.1016/j.jhazmat.2024.135894.
Wang, Y., Xu, J., Liu, Z., Cui, H., Chen, P., Cai, T., Li, G., Ding, L., Qiao, M., Zhu, Y., Zhu, D., 2024b. Biological interactions mediate soil functions by altering rare microbial communities. Environ. Sci. Technol. 58 (13), 5866–5877. https://doi.org/10.1021/acs.est.4c00375.
Wang, Y., Zhan, W., Ren, Q., Cheng, S., Wang, J., Ma, X., Zhang, C., Wang, Y., 2019. Biodegradation of di-(2-ethylhexyl) phthalate by a newly isolated *gordonia* sp. and its application in the remediation of contaminated soils. Sci. Total Environ. 689, 645–651. https://doi.org/10.1016/j.scitotenv.2019.06.459.
Wang, Y., Zhao, Y., Bollas, A., Wang, Y., Au, K.F., 2021. Nanopore sequencing technology, bioinformatics and applications. Nat. Biotechnol. 39 (11), 1348–1365. https://doi.org/10.1038/s41587-021-01108-x.
Wu, E., Chen, H., Tang, L., Zeng, L., Ji, H., Zhu, M., 2024a. Molecular understanding on ultraviolet photolytic degradation of cyano liquid crystal monomers. J. Hazard. Mater. 465, 133033. https://doi.org/10.1016/j.jhazmat.2023.133033.
Wu, J., Bian, C., Yang, X., Su, G., 2025a. CytoToxLCM: a software to predict cytotoxicity of emerging contaminant liquid crystal monomers. Environ. Sci. Technol. 59 (14), 7028–7038. https://doi.org/10.1021/acs.est.5c00027.
Wu, J., Lv, D., Lin, W., Mao, Y., Xia, Y., Feng, L., Zhao, T., Mao, X., Shu, F., Guo, H., 2025b. Chronic exposure to liquid crystal monomer EBCN at environmentally relevant concentrations induces testicular dysfunction via the gut-testis axis. J. Hazard. Mater. 486, 137033. https://doi.org/10.1016/j.jhazmat.2024.137033.
Wu, J., Ye, W., Feng, Y., Lao, W., Li, J., Lu, H., Liu, G., Su, G., Deng, Y., 2024b. Aquatic photolysis of high-risk fluorinated liquid crystal monomers: kinetics, toxicity evaluation, and mechanisms. Water Res. 255, 121510. https://doi.org/10.1016/j.watres.2024.121510.
Wu, Y., Yang, T., Wu, Y., Liang, Y., Zeng, X., Yu, Z., Peng, P.A., 2024c. Co-metabolic biotransformation of bisphenol AF by a bisphenol a-growing bacterial enrichment culture. Environ. Sci. Technol. 58 (51), 22799–22807. https://doi.org/10.1021/acs.est.4c10861.
Wu, Y., Zhu, M., Ouyang, X., Qi, X., Guo, Z., Yuan, Y., Dang, Z., Yin, H., 2024d. Integrated transcriptomics and metabolomics analyses reveal the aerobic biodegradation and molecular mechanisms of 2,3′,4,4′,5-pentachlorodiphenyl (PCB 118) in *methylorubrum* sp. ZY-1. Chemosphere 356, 141921. https://doi.org/10.1016/j.chemosphere.2024.141921.
Xie, J., Wei, G., Zeng, L., Liu, L., 2024. Liquid crystal monomers in soils near the e-waste recycling site and liquid crystal display manufacturer: exponential decrease with distance. Sci. Total Environ. 909, 168428. https://doi.org/10.1016/j.scitotenv.2023.168428.
Xing, H., Yu, X., Sun, J., Lu, G., Zhu, M., Liang, J., Jin, L., Zhu, L., 2023. Interaction between phthalate ester and rice plants: novel transformation pathways and metabolic-network perturbations. Environ. Sci. Technol. 57 (24), 8870–8882. https://doi.org/10.1021/acs.est.2c09737.
Xu, G., Liu, X., Han, J., Shao, K., Yang, H., Yuan, J., Dou, J., 2025a. Insights into the enhanced uranium reduction efficiency through extracellular polymeric substances from *Desulfovibrio vulgaris* UR1 induced by mediating materials. Bioresour. Technol. 421, 132143. https://doi.org/10.1016/j.biortech.2025.132143.
Xu, L., An, X., Jiang, H., Pei, R., Li, Z., Wen, J., Pi, W., Zhang, Q., 2025b. A novel *gordonia* sp. PS3 isolated from the gut of *galleria mellonella* larvae: mechanism of polystyrene biodegradation and environmental toxicological evaluation. J. Hazard. Mater. 488, 137219. https://doi.org/10.1016/j.jhazmat.2025.137219.
Xue, Y., Chen, H., Yang, J.R., Liu, M., Huang, B., Yang, J., 2018. Distinct patterns and processes of abundant and rare eukaryotic plankton communities following a reservoir cyanobacterial bloom. ISME J. 12 (9), 2263–2277. https://doi.org/10.1038/s41396-018-0159-0.
Zelezniak, A., Andrejev, S., Ponomarova, O., Mende, D.R., Bork, P., Patil, K.R., 2015. Metabolic dependencies drive species co-occurrence in diverse microbial communities. Proc. Natl. Acad. Sci. 112 (20), 6449–6454. https://doi.org/10.1073/pnas.1421834112.
Zhang, J., Li, X., Klumper, U., Lei, H., Berendonk, T.U., Guo, F., Yu, K., Yang, C., Li, B., 2022a. Deciphering chloramphenicol biotransformation mechanisms and microbial interactions via integrated multi-omics and cultivation-dependent approaches. Microbiome 10 (1), 180. https://doi.org/10.1186/s40168-022-01361-5.
Zhang, J., Zhu, M., Ouyang, X., Yuan, Y., Tang, S., Yin, H., 2025a. Co-metabolism degradation of tetrabromobisphenol A by the newly isolated *sphingobium* sp. strain QY1-1: multiple metabolic pathways, toxicity evaluation, and mechanisms. J. Hazard. Mater. 488, 137440. https://doi.org/10.1016/j.jhazmat.2025.137440.
Zhang, R., Zhang, X., Zhang, Q., Li, Y., Wang, Y., Xu, J., Cheng, Z., Chen, H., Yao, Y., Sun, H., 2024. Heterogeneous photodegradation behavior of liquid crystal monomers in dust: quantitative structure–activity relationship and product identification. Environ. Sci. Technol. 58 (8), 3908–3918. https://doi.org/10.1021/acs.est.3c04753.
Zhang, S., Cheng, Z., Zhang, T., Ding, Y., Zhu, H., Wang, L., Sun, H., 2025b. Liquid crystal monomers induce placental development and progesterone release dysregulation through transplacental transportation. Nat. Commun. 16, 1204. https://doi.org/10.1038/s41467-025-56552-z.
Zhang, Y., Mao, G., Liu, R., Zhou, X., Bartlam, M., Wang, Y., 2022b. Transcriptome profiling of *Stenotrophomonas* sp. Strain WZN-1 reveals mechanisms of 2,2′,4,4′-tetrabromodiphenyl ether (BDE-47) biotransformation. Environ. Sci. Technol. 56 (16), 11288–11299. https://doi.org/10.1021/acs.est.2c00197.
Zhao, J., Brandt, G., Gronniger, J.L., Wang, Z., Li, J., Hunt, D.E., Rodriguez-R, L.M., Hatt, J.K., Konstantinidis, K.T., 2025a. Quantifying the contribution of the rare biosphere to natural disturbances. ISME J. 19 (1), wraf129. https://doi.org/10.1093/ismejo/wraf129.
Zhao, W., Wu, Y., Fu, C., Li, L., 2025b. Mutualistic cross feeding mediated by metabolic intermediates and siderophores enhances dibenzo-p-dioxin removal. Environ. Sci. Technol. 59 (28), 14508–14517. https://doi.org/10.1021/acs.est.4c11857.
Zhou, Z., Li, M., Xu, J.H., Zhang, Z.J., 2018. A single mutation increases the activity and stability of *ectobacterium carotovorum* nitrile reductase. Chembiochem 19 (5), 521–526. https://doi.org/10.1002/cbic.201700609.
Zhu, X., Yu, Y., Meng, W., Huang, J., Su, G., Zhong, Y., Yu, X., Sun, J., Jin, L., Peng, P.A., Zhu, L., 2024. Aerobic microbial transformation of fluorinated liquid crystal monomer: new pathways and mechanism. Environ. Sci. Technol. 58 (1), 510–521. https://doi.org/10.1021/acs.est.3c04256.